Sensitivity Analysis of Optical Metrics for Spectral Splitting Photovoltaic Systems: A Case Study

David Berney Needleman, Jonathan P. Mailoa, Riley E. Brandt, Niall M. Mangan, and Tonio Buonassisi, *Member, IEEE*

***Abstract*— Spectral splitting of sunlight to increase photovoltaic efficiency beyond the Shockley-Queisser limit has gained interest in recent years. Sensitivity analysis can be a useful tool for system designers to determine how much deviation from ideal conditions can be tolerated for different optical parameters. Understanding the origin of these sensitivities can offer insight into materials and device design. We employ 2-D TCAD simulations to analyze the sensitivity of system performance to two optical parameters: spectral fidelity (the fraction of photons directed to the intended material), and the spatial uniformity of illumination intensity. We analyze a system using crystalline silicon (Si) and cuprous oxide (Cu_2O) as absorbers. We find that the spectral fidelity of the light directed to the Si cell has to be greater than 90% for the system to outperform a high-efficiency single-junction Si device. Varying the fidelity of the light directed to the Cu_2O cell from 55% to 90% changes system efficiency by less than 10% relative. In some cases, increasing the fidelity of this light reduces system efficiency. We find no significant impact of spatial variation on length scales from 600 µm to 4.8 mm in devices with emitter sheet resistance less than 500 Ω/□.**

***Index Terms*— Photovoltaic systems, semiconductor device modeling, spectral splitting, optical system design.**

I. Introduction

SPECTRAL splitters have great potential to increase photovoltaic (PV) system efficiency by guiding photons to matched absorber materials, increasing the amount of the solar spectrum that can be absorbed and reducing thermalization losses. Simultaneous development of high-efficiency solar cells using absorbers with a wide range of band gaps [1], [2] and computational optics enabling novel optical components has increased the interest in and efficiency of spectral splitting PV [3]–[8]. However, the current record efficiency of 38.7% falls short of both theoretical efficiency limits for 4-junction devices and the summed efficiency of the component devices. Some of this deficit can be attributed to optical losses.

Optical system designers benefit from a framework to evaluate the most important loss mechanisms in spectral splitting systems. Many efforts have been made and tools developed to optimize spectral splitting systems (*e.g.*, [9]–[11]), which provides guidance on ideal system configuration and loss mechanism. Analyzing the sensitivity of system performance to optical parameters can provide valuable insight into which optical parameters must be tightly controlled and which can be relaxed. Understanding the origin of these sensitivities can also indicate the important material and device design parameters for spectral splitting PV.

Russo *et al.* introduced a set of universal metrics for evaluating the quality of spectral splitting optics in an effort to homogenize the analysis of spectral splitting PV systems [12]. Optical metrics enable the evaluation of optical components of spectral splitting PV systems in the same way that metrics like quantum efficiency are used to analyze solar cell devices. Since a major advantage of spectral splitting PV is the partial decoupling of the optical and electrical systems, having independent metrics for the optical system is useful. Recently, Russo *et al.* used their analytical framework to present a sensitivity analysis of several variables related to the form factor and positioning of dispersive spectral splitting systems [13]. Understanding system sensitivities to optical metrics enables optical system designers to develop systems without the need for constant simulation or measurement of devices and moves toward design rules that are independent of specific solar cell characteristics.

To further demonstrate the utility of sensitivity analysis so that it will be used more broadly, we perform a sensitivity analysis for two different parameters for spectral splitting optics. The first, which we call *spectral fidelity*, measures the precision with which the solar spectrum is split. System efficiency shows a strong sensitivity to spectral fidelity, implying that it must be tightly controlled. The second is the spatial uniformity of light intensity over the surface of a solar

Manuscript received September 16, 2014. Support was provided by the Assistant Secretary of Defense for Research & Engineering under Air Force Contract number FA8721-05-C-0002; a National Science Foundation (NSF) grant for Energy, Power, and Adaptive Systems under Contract number ECCS-1102050; and the National Research Foundation Singapore through the Singapore MIT Alliance for Research and Technology's Low Energy Electronic Systems research program. D. Berney Needleman and Riley E. Brandt acknowledge the support of the Department of Defense (DoD) and the NSF through the National Defense Science & Engineering Graduate Fellowship (NDSEG) program and National Science Foundation GRFP fellowship, respectively.

All authors are with the Massachusetts Institute of Technology, Cambridge, MA 02139 USA (emails: dbn@mit.edu, buonassisi@mit.edu).

cell. System efficiency shows a weak sensitivity to spatial uniformity, implying that deviation from the optimal value can be tolerated for this combination of devices under 1 sun illumination.

To rigorously analyze the effect of injection level- and wavelength-dependent conversion efficiency, we perform our sensitivity analysis with a full 2-D TCAD package. These effects cannot be accounted for with the diode equation-based approaches typically used in optimization routines. Notably, for the parameters and systems we analyzed, injection and wavelength-dependent effects were small compared to changes in current. To maintain consistency between the simulations for the two parameters, 2-D simulations, which were required for analyzing spatial uniformity, were used for both. Our results indicate when 1-D simulations are suitable despite spatial variation in illumination intensity.

II. Optical Parameters

A. Spectral Fidelity

One important property of optical components for spectral splitting PV is the precision with which the optical system divides the incident spectrum. To quantify this property, we define spectral fidelity as the fraction of photons in the wavelength range intended for a given sub-cell that are actually directed to that sub-cell:

$$f_k = \frac{\int_{\lambda_{k1}}^{\lambda_{k2}} \Phi_k(\lambda)d\lambda}{\int_{\lambda_{k1}}^{\lambda_{k2}} \Phi_{incident}(\lambda)d\lambda} \quad [1]$$

Where λ_{k1} and λ_{k2} define the wavelength range of a spectral band ideally directed toward the kth sub-cell, $\Phi_{incident}$ is the photon flux as a function of wavelength incident on the optical component, and Φ_k is the photon flux that is actually directed to the kth sub-cell. In our system, k=1 corresponds to the Cu_2O cell and k=2 corresponds to the Si cell.

The concept that splitting precision affects system efficiency has been highlighted in previous work [2], [7], [9], [11], [13]–[17]. We introduce spectral fidelity as a way to quantify this precision in a generic way applicable to many optical components. Spectral fidelity is similar to the optical transfer efficiency defined by Russo *et al*. in [12], [13], but it is based on the number of incident photons as a function of wavelength rather than the incident energy. As the energy per photon has little effect on either the device current or the voltage at which electrons are collected, we prefer the spectral fidelity metric. We further expand on their work by performing a sensitivity analysis of this variable and determining the relative importance of the fidelity of each spectral band.

In our tandem system, we define the high-energy spectral band (the wavelength range ideally directed to the first sub-cell) as $\lambda \geq 605$ nm, corresponding to the band gap of Cu_2O, and the low-energy spectral band (the wavelength range ideally directed to the second sub-cell) as $\lambda < 605$ nm. Note that because spectral fidelity for each spectral band only counts the photons within the selected wavelength range for that spectral band, the fidelity of each spectral band is independent, and the sum of the fidelities does not have to equal 100%.

We simulate a range of fidelities, using the following method to generate appropriate spectra: First, we split the solar spectrum perfectly (Fig. 1a). Then, we apply a Gaussian decay function (dashed blue lines in Fig. 1b) to the high-energy spectral band and the complement of that function (dashed red lines in Fig. 1b) to the low-energy spectral band. We fit the decay constants and center of the decay function using a least squares method to achieve the desired fidelity of each spectral band.

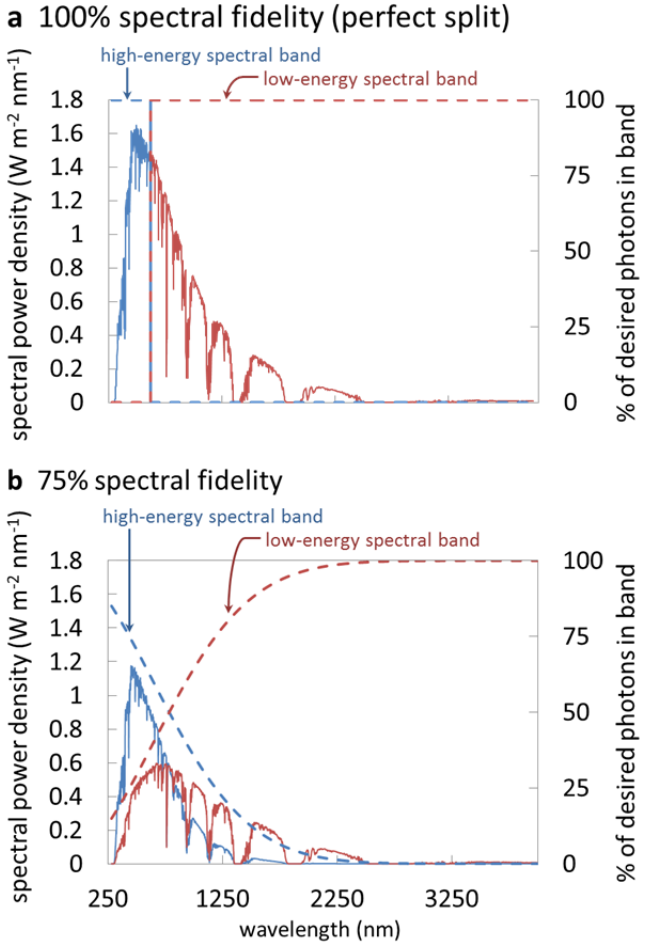

Fig. 1. Spectral fidelity illustrated. Splitting functions with Gaussian decay and its complement (dashed lines, right axis) and spectral power density (solid lines, left axis) *vs.* wavelength (horizontal axis) when splitting functions are applied to AM 1.5G solar spectrum. a) Perfect split. b) 75% fidelity in both spectral bands.

We use Gaussian decay near the cut-off wavelength because we assume that leakage from one spectral band to the other would be most pronounced in this spectral range. In other words, we assume the edges of our spectral bands are not perfectly sharp. The use of complementary functions ensured that photon flux (and therefore incident power) as a function of wavelength is conserved. It also implies that the optical system is lossless (all incident photons arrive at one sub-cell or the other). The resulting spectra for 75% fidelity in both bands are shown in Fig. 1b. In addition to perfect splitting, we simulate all combinations of 55%, 65%, 75%, 85%, and 90%

fidelity in each spectral band.

B. Spatial Uniformity

We simulate a Gaussian variation in light intensity over the surface of the device. Gaussian variation is realistic for many optical systems and allows for simple, intuitive characterization of the variation using the coefficient of variance (*CV*), the ratio of the standard deviation to the mean, where the mean is taken to be the full simulation width.

The method for generating Gaussian variation in intensity is as follows: First, we split the spectrum into spectral bands with the desired fidelity, as described above. Then, we generate a discrete normal distribution of twenty-one points across the surface of the device. We normalize this distribution so that the total photon flux across the entire surface remains constant at an intensity of one sun. We then multiply the values of the normal distribution by the split spectra, generating twenty-one discrete spectra to apply across the surface of the device.

Values of CV = 0.009, CV = 0.091, and CV = 0.909 are tested. The corresponding maximum and minimum intensities are 1.1 and 0.7 suns for CV = 0.909, 8.4 and 1.6×10^{-21} suns for CV = 0.091, and 21 and 0 suns for CV = 0.009, with the intensity going to 0 suns at approximately 64% of the mean (full simulated width).

III. Materials Selection

The value of and lessons from sensitivity analysis are generalizable. However, realistic simulations require optical and electronic properties based on real materials. We simulate devices with Si and Cu_2O absorbers. We chose Si as an absorber material because it is non-toxic, abundant [18], high-efficiency, low-cost, has a proven track-record in the field [19], and comprises more than 90% of the PV market [20]. Using the method of Henry [21], we performed a detailed balance calculation to determine the best band gap for a tandem cell paired with Si, and found Cu_2O to be almost ideal (2.05 eV *vs.* 1.9 eV ideal). Furthermore, Cu_2O is also non-toxic and abundant [22]. Most materials currently used in multijunction solar cells, like III-V compounds, are not abundant enough to produce tens of TW of power [23]. One of the key advantages of spectral splitting rather than stacked multijunction devices is that it enables consideration of a broader range of semiconductors by removing the need for lattice matching and epitaxial growth. We therefore feel consideration of more scalable materials like Cu_2O is a compelling research priority.

We simulate Cu_2O devices significantly more efficient than current records, as described below in the TCAD Simulations section. We feel Cu_2O is a reasonable material choice despite this necessity for several reasons. First, the idealized properties for Cu_2O are similar to those of other high-performance semiconductors with a band gap near 2 eV, like GaP or InGaP, and these simulations can generalize to those for other high-efficiency wide-gap semiconductors. The relatively gradual onset of absorption in our Cu_2O model also enables us to demonstrate the importance of quantum efficiency as described in the Results section. Second, the record efficiency of Cu_2O devices has increased by 44% since 2011 [24] and 364% since 2005 [25], and there are several examples of other material systems, most recently metal-halide perovskites, doubling their efficiency or increasing it by more than 5% absolute over a short period [26]. Furthermore, each of our simulated parameters are similar to values in the literature. We simulate open-circuit voltages (V_{OC}) of 1.2 – 1.3 V, minority carrier lifetimes of 8 – 600 ns , and mobilities of 30 – 100 $cm^2/V{\cdot}s$. Values for each of these parameters of 1.2 V [27], 10 µs [28], and 62 $cm^2/V{\cdot}s$ (measured by Hall effect) [29], respectively, have been reported. Controllable doping [30], and good contact formation [31] have also been demonstrated.

IV. TCAD Simulations

We simulate Si and Cu_2O devices using the Sentaurus Device TCAD software package and calculate the total system efficiency assuming a 4-terminal architecture. We simulate one higher-efficiency and one lower-efficiency architecture for both Si and Cu_2O. For Si, we simulate a standard *p*-type diffused-junction device with an AM 1.5G efficiency of 19.4%, representing the performance of a high-end turnkey line [20]. We also simulate a passivated emitter rear totally-diffused (PERT) cell [32]–[34] with AM 1.5G efficiency (24.0%) similar to the best commercially-available solar cells [35], [36]. The unit cell for our simulations is the smallest distance between two lines of symmetry, from the mid-point of one contact halfway to the next contact.

A Cu_2O device must have an AM 1.5G efficiency greater than about 10% for a Cu_2O-Si tandem device to outperform Si alone [37]. Therefore, though the current record efficiency for Cu_2O is 5.4% [38], we simulate devices with AM1.5G efficiencies of 11.6% and 13.7%. 13.7% is near the theoretical limit for a heterojunction solar cell with the conduction band offset of Cu_2O and zinc oxide but otherwise ideal material properties. For both devices, we simulate a heterojunction with Cu_2O and zinc oxysulfide, using idealized minority carrier lifetime and mobility and conduction band alignment. For more details on the simulation parameters, see [39].

For the Si simulations without spatially varying illumination, we use Sentaurus's built-in transfer-matrix-method (TMM) optical solver. Spectra with different fidelities as described above are used as the input to the TMM solver.

For spatially varying illumination, because the thickness and the width of the silicon devices simulated are much greater than all wavelengths of incoming light, the silicon device is modeled using geometrical optics in MATLAB. Monocrystalline silicon devices are typically textured into pyramids with a facet angle to the horizontal of 54.4°. Light was assumed to be normally incident, strike one of these facets, and be refracted based on a constant index of refraction. We assume any photons that reached the back surface are perfectly reflected and any photons that subsequently reach the front surface escape. Because only 2% of incident photons reached the front surface after being

reflected off the back, the effect of multiple scattering paths is considered to be negligible and omitted to reduce computation time. A wavelength-dependent absorption coefficient is convoluted with the path vector to determine absorption as a function of position.

Since the thickness (and in some cases the width) of the Cu_2O devices simulated is on the order of the wavelength of solar illumination, optical simulations for both uniform and spatially varying illumination are performed using the finite-difference time-domain (FDTD) method with a repeating surface texture experimentally obtained from a representative atomic force micrograph of a real Cu_2O device and periodic boundary conditions. More details on the FDTD simulations can be found in [40].

The procedure for inputting carrier generation profiles for non-uniform illumination is discussed in detail in [31]. We include a brief overview here: First, we discretize the device across its width. We then perform the optical simulations as described above, illuminating each discretized region one at a time. The intensity of the illumination varies with the Gaussian intensity distribution across the width of the device described above in the Spatial Uniformity section. Note that illumination on a discrete region generates carriers over the full device width due to reflection and scattering. We implicitly assume that the interaction of these scattered and reflected photons with those from illumination of different regions of the device is negligible.

Next, the total generation rates from illumination of each portion of the device are linearly combined to calculate the total generation rate as a function of position. Then, we average the generation rate across the width of each discretized region to obtain 1-D generation profiles as a function of depth for each region. In each Sentaurus simulation, we generate the device structure so that the base of the solar cell has corresponding discrete spatial "regions" across its width. We then interpolate each of the 1-D profiles across the appropriate region.

V. Results and Discussion

A. Spectral Fidelity

Fig. 2 shows the sensitivity of the total system efficiency (contours, color scale) to the fidelity of the high-energy spectral band (the fraction of photons with energy greater than the band gap of Cu_2O directed to Cu_2O, plotted on the *x*-axis) and the fidelity of the low-energy spectral band (the fraction of photons with energy less than the band gap of Cu_2O directed to Si, *y*-axis). Simulated data points are indicated with filled circles and the contour lines are interpolated between these points. Fig. 2a contains data for the most efficient pairing: a high-efficiency Cu_2O device and a high-efficiency Si device. Fig. 2b contains data for the combination of devices with the most similar efficiency: high-efficiency Cu_2O and low-efficiency Si.

For comparison, the efficiency of the Si devices under AM 1.5G illumination are also plotted (black contour lines). Low-efficiency Si is not plotted in Fig. 2a, since if the system cannot out-perform one of its components (high-efficiency Si), spectral splitting is clearly not beneficial. However, combining low-cost Si devices with lower-efficiency wide-gap semiconductors has been considered as a low-cost alternative to single-junction devices with more expensive materials. Therefore, the performance of high-efficiency Si is plotted for reference in Fig. 2b.

The large variation in efficiency coupled with the relatively flat contours indicates the importance of the low-energy spectral band fidelity and the lack of importance of high-energy spectral band fidelity. For the high-efficiency pairing (Fig. 2a), the efficiency is only better than Si alone (black contour line) when the low-energy spectral band fidelity is greater than 85 – 90%, depending on the high-energy spectral band fidelity. When the efficiencies of the wide-gap and narrow-gap devices are more similar (Fig. 2b), the system is slightly more robust to lower fidelity in the low-energy spectral band. However, low-energy spectral band fidelity of about 75 – 85% is still required for the system to outperform low-efficiency Si alone (lower black contour line), and low-energy spectral band fidelity greater than 95% is required for better performance than high-efficiency Si alone (higher black contour line).

The greater importance of low-energy spectral band fidelity makes sense because low-energy photons directed to the wide-gap material are not absorbed, so all of their energy is lost, while high-energy photons directed to the narrow-gap material are absorbed, so only a fraction of their energy is lost to thermalization. Considered another way, there is a one-to-one correlation between fidelity losses in the low-energy spectral band and photocurrent losses. A one-to-one loss in current must result in at least a one-to-one loss in efficiency, as per the standard definition of efficiency, η:

$$\eta = \frac{J_{SC} \times V_{OC} \times FF}{P_{Solar}} \qquad [2]$$

If the common approximation that the short-circuit current (J_{SC}) equals the photocurrent is used, the loss of absorption is directly proportional to the loss in efficiency. V_{OC} usually decreases (logarithmically) with the photocurrent (approximated as J_{SC}), further exacerbating these losses. In contrast, losses in fidelity in the high-energy spectral band only result in sub-linear changes in V_{OC} due to thermalization losses in the narrow-gap material.

The importance of non-absorption is demonstrated in Fig. 3 by comparing the normalized efficiency (system efficiency for given fidelities divided by the system efficiency under perfect splitting) to normalized J_{SC} (sum of the J_{SC} for each sub-cell for given fidelities divided by the sum of the J_{SC} under perfect splitting) for every pair of devices with every combination of fidelities. A perfect 1:1 correlation (the black line in the figure) would indicate that all of the losses are current losses and therefore due to reduced absorption. The data fall very close to this line for all combinations of fidelities and all pairs of devices. The deviations, particularly at extremely low and high values of normalized J_{SC}, are largely due to variations in

the average voltage at which carriers are extracted from the system. This value depends on the fraction of total current produced by the wide-gap or narrow-gap device, which is in turn a function of the fidelity of both spectral bands.

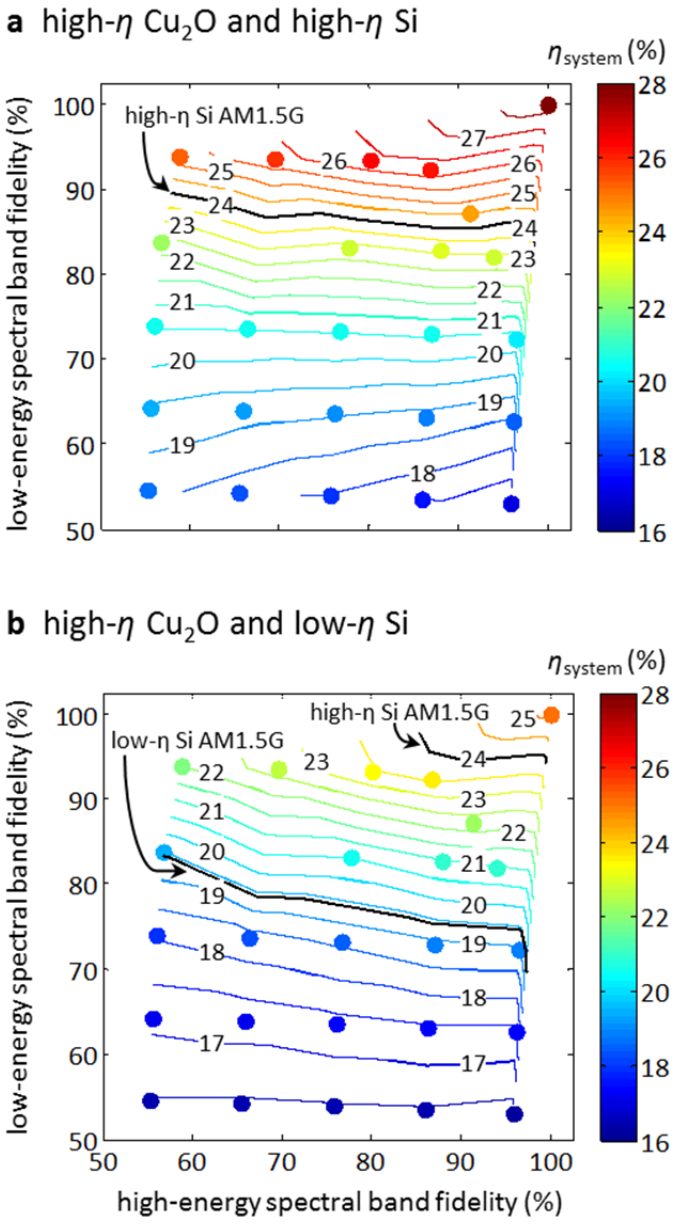

Fig. 2. System efficiency is sensitive mostly to fidelity of the low-energy spectral band. System efficiency (contour, color) plotted *vs.* fidelity of the high-energy spectral band (directed to Cu_2O, *x*-axis) and fidelity of the low-energy spectral band (directed to Si, *y*-axis). Values of Si sub-cell AM 1.5G efficiency (black contour lines) for both high-efficiency Si and low-efficiency Si (2b only) devices are shown for comparison. Filled circles represent pairs of fidelity values simulated and contours are interpolated between them using a cubic spline function. a) High-η Cu_2O and high-η Si. b) High-η Cu_2O and low-η Si.

The importance of absorption was also highlighted by results recently reported by Eisler *et al*. [41]. The authors demonstrated that the maximum efficiency of multijunction devices is achieved by maximizing conversion not only of solar photons but also of photons radiated from wide-band gap cells. In some cases, increased absorption of these radiated photons led to higher efficiencies than increasing the number of sub-cells (*i.e.*, reducing the thermalization losses).

Under certain regimes, increased fidelity of the high-energy spectral band is detrimental to total system efficiency. This effect appears as contours sloping up from left to right in Fig. 2 and indicates that it is sometimes beneficial to absorb high-energy photons with a narrower-gap material (Si). The effect is seen most clearly in the figure at low values of low-energy spectral band fidelity and high values of high-energy spectral band fidelity. We attribute it to low external quantum efficiency (*EQE*) at longer wavelengths of the Cu_2O devices simulated. Cu_2O, like many semiconductors, has a distinct slope in its *EQE* curve near its band edge [40], so the system loses current by directing 500 – 620 nm photons to the Cu_2O cell. The increased voltage per electron collected by the Cu_2O rather than the Si cell is not always sufficient to make up for the current loss. For the lower-efficiency Si device, the voltage benefit is greater, so the wavelength range over which the current loss dominates is smaller. The slope of the system efficiency contours on a spectral fidelity map therefore provides a way to verify if the wavelength ranges chosen to define spectral fidelity correspond to "perfect" splitting (*i.e.*, if they maximize efficiency). In our case, we see that it is not, as assumed here, at the band edge of Cu_2O. Another approach to determining the wavelength ranges for perfect splitting is to use the cross-over point for the spectral conversion efficiency, as defined by Russo *et al*. [13]. However, this method neglects the injection-level and absorption profile dependence of voltage. Both methods suggest a design strategy for optical systems based on relative cell EQEs rather than band gap.

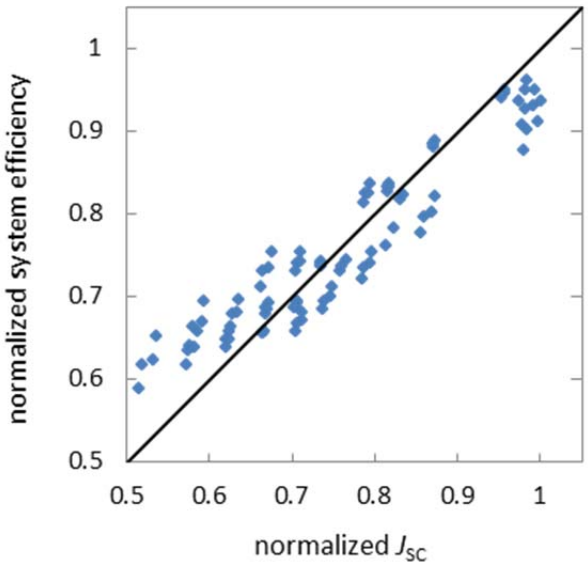

Fig. 3. Nearly 1:1 correlation between normalized efficiency and normalized J_{SC}. Data include every combination of fidelities and every combination of high- and low-efficiency devices. Efficiency and J_{SC} are normalized for each point to the efficiency and J_{SC} of the same pair of devices under illumination by a perfectly split spectrum (100% fidelity in both spectral bands). Line shows a 1:1 correlation between current loss and efficiency loss.

Changes in device parameters like minority carrier lifetime and mobility can affect the injection-dependence of efficiency.

There might be concern that such differences in the injection-dependent performance of low-efficiency devices compared to high-efficiency devices contribute strongly to the change in sensitivity between Fig. 2a and Fig. 2b. To test this hypothesis, we vary the fidelity of the spectral band directed toward a given sub-cell, while keeping the fidelity of the other spectral band constant at 90%, as shown in Fig. 4. The performance of high- and low-efficiency devices relative to their performance under perfect spectral splitting is nearly identical at all fidelity values for both Si and Cu_2O. We therefore rule out differences in individual sub-cell performance as a cause of the changes in the impact of fidelity for different pairs of devices.

Given the demonstrated importance of current losses, we attribute the similarity in the relative performance of high- and low-efficiency devices to the high rate of carrier collection of all the devices simulated. It therefore appears that the most important reduction in *EQE* at long wavelengths are related to decreased absorption rather than decreased carrier collection. The difference in the slopes of the Si and Cu_2O curves in Fig. 4 are also almost entirely due to differences in J_{SC} losses. The origin of this difference is again the poor *EQE* of Cu_2O at longer wavelengths, which means that many of the photons redirected from the Cu_2O to the Si would not have been converted by the Cu_2O anyway.

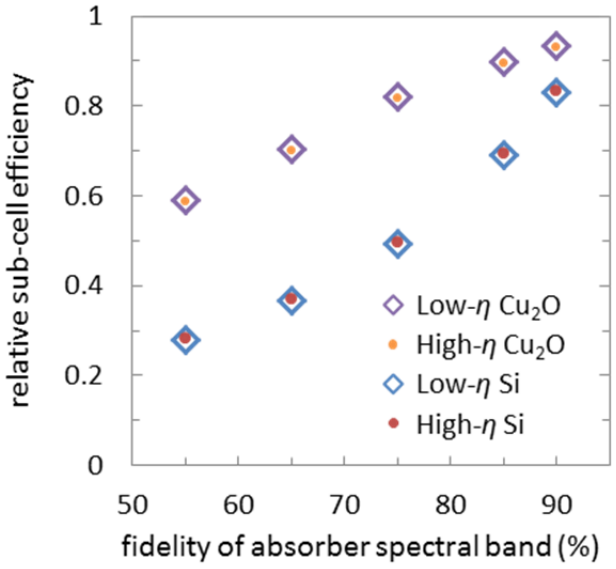

Fig. 4. No difference between response of high-η and low-η devices to varying fidelity. Sub-cell efficiency of higher and lower-efficiency Si and Cu_2O devices, normalized to the efficiency of the respective device at 100% fidelity plotted *vs.* fidelity of the spectral band intended for the given absorber (low-energy spectral band for Si and high-energy spectral band for Cu_2O). The other spectral band fidelity was kept constant at 90%.

B. Spatial Uniformity

We find that spatial uniformity of the incident light intensity, has virtually no effect on efficiency, internal quantum efficiency (*IQE*), or V_{OC}. We vary the *CV* of a Gaussian distribution of intensity with an average intensity of 1 sun on length scales between 600 and 4800 µm for c-Si devices and between 1 and 100 µm for Cu_2O devices. These length scales were chosen to span values significantly less than the minority-carrier diffusion length to values significantly higher. For the Si simulations, they vary from one third to three times the minority-carrier diffusion length. For the high-efficiency Cu_2O simulations, they vary from one twelfth to 8 times, and for the low-efficiency Cu_2O simulations, from 1.25 to 125 times. These length scales are also on the order of the intensity variation produced by some spectral splitting optical components, for example, diffractive optics [42], [43]. Fig. 5 plots the device performance metrics (normalized to the value for uniform illumination) for different values of *CV* and different length scales of the spatial variation. The error bars indicate the variation in output parameters attributed to changes in light intensity due to the way the variation is introduced into Sentaurus Device [39]. While we show results only for a c-Si device with a diffused emitter at 100% fidelity, similarly insignificant impact is observed for all Si and Cu_2O devices at both 100% and 55% fidelity.

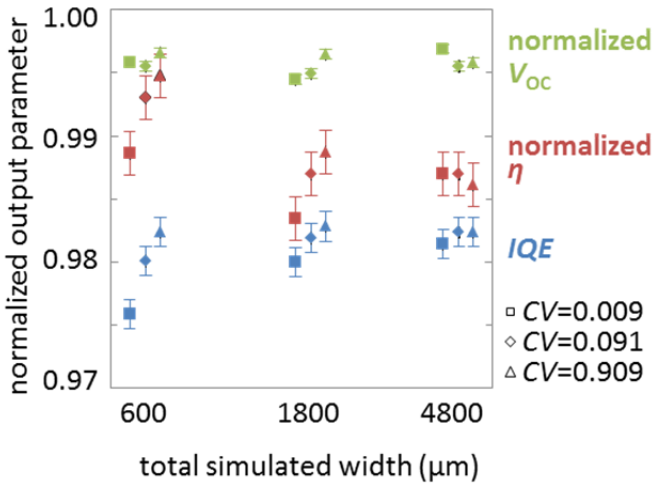

Fig. 5. Spatial uniformity has little impact on Si diffused junction device performance. Simulated performance metrics, efficiency, V_{OC}, and J_{SC}, plotted *vs.* simulation width. The data series for each width is the *CV*, varying from 0.007 to 0.442. Data shown for 100% fidelity. All devices had similarly insignificant sensitivity to spatial intensity variations at both 100% and 55% fidelity.

The relative insignificance of spatial variation of light intensity is further demonstrated in Fig. 6. Here the losses in total system efficiency relative to uniform illumination and perfect splitting are plotted *vs. CV* for a combination of high-efficiency Cu_2O and low-efficiency Si. Each data series represents a different fidelity value, with the fidelity of the two spectral bands equal to each other and varied together. The flat slopes indicate the unimportance of spatial variation compared with spectral fidelity.

It might be expected that lateral carrier redistribution beyond the bulk minority-carrier diffusion length (~1600 µm for the simulations in Fig. 5) would not occur, leading to local regions of lower current and voltage. However, it has been observed previously that low-resistivity emitters offer a much more efficient conduction path than the bulk and enable transport over much longer distances [44]. Our simulations

show that near open-circuit conditions, lateral current flow in the emitter indeed redistributes carriers from regions of high illumination intensity to regions of low illumination intensity. This redistribution current is driven by a lateral voltage drop in the device due to non-uniform carrier generation. However, because relatively little current is required to redistribute carriers in these non-concentrating simulations and the emitter resistance is low, the power loss due to this voltage drop is small. These results help explain why earlier work also found little effect from non-uniform illumination under low concentration [42].

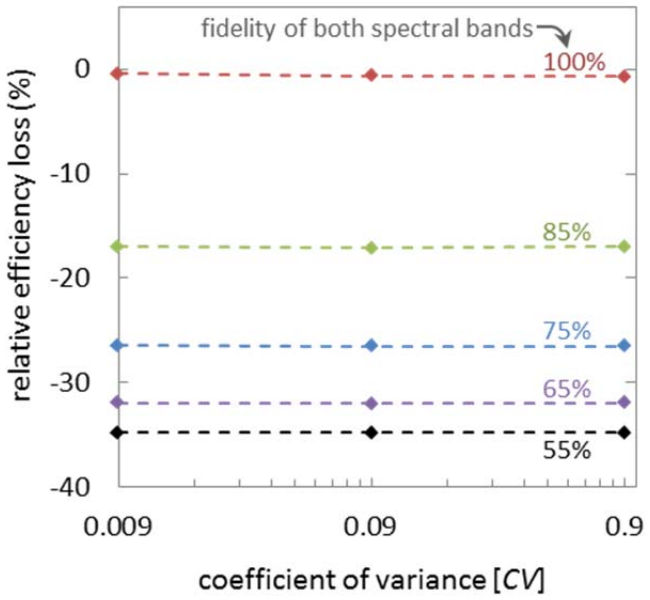

Fig. 6. Insignificance of spatial variation compared with spectral fidelity. The reduction in total system efficiency relative to the efficiency under uniform illumination with perfect splitting is plotted *vs. CV* for a range of fidelity values. The fidelities were the same in both spectral bands and the results shown are for a combination of high-efficiency Cu_2O and low-efficiency Si.

We test the hypothesis that high emitter conductivity is eliminating effects of spatial inhomogeneity by simulating a 600 μm-wide diffused-junction Si device with increased emitter sheet resistance. We reduce the peak emitter doping concentration from its original value of 6×10^{19} cm^{-3} to a range from 5×10^{16} to 1×10^{19} cm^{-3}. We also reduce the depth of the emitter diffusion. For the original simulation the characteristic length of the Gaussian doping profile is 150 nm, while for the high sheet resistance simulations, it is 100 nm. To maintain a reasonable V_{OC}, it is necessary to maintain the built-in voltage of the junction. To accomplish this, we simultaneously decrease the base doping concentration to achieve maximum efficiency for a given emitter doping. Base doping is decreased from 2×10^{16} cm^{-3} in the original simulations to 5×10^{15} cm^{-3}. For a peak doping concentration of 1×10^{19} cm^{-3}, this device has a simulated efficiency under uniform illumination of 11.5% with a J_{SC} of 21.43 mA/cm^2, V_{OC} of 0.651 V, and *FF* of 82.1%. Note that the efficiency of the devices is reduced by reducing the emitter doping concentration. We account for this reduction by considering a normalized efficiency, the ratio of efficiency under spatially varying illumination to that under uniform illumination.

Fig. 7 shows the effect of sheet resistance on efficiency under illumination by a perfectly split spectrum with a *CV* of 0.009. The reduction in efficiency does not increase until the emitter doping concentration is less than 10^{19} cm^{-3}. This corresponds to a sheet resistance of 494 Ω/□, compared with 87 Ω/□ for the original simulation. The saturation of the efficiency reduction at about 1% is most likely due to a competing effect like greater emitter recombination due to higher doping. These results are qualitatively similar to those observed under concentrated light by García *et al.* [44]. Indeed, the importance of low emitter sheet resistance to allow lateral current flow in systems with non-uniform illumination has long been established, even for non-concentrating solar cells [45], [46]. Existing high-resistivity metal pastes are designed for 100–120 Ω/□ emitters and light diffusions in PERT and PERL structures are on the order of 400–500 Ω/□. While we highlight the lack of sensitivity in the more realistic devices in this work, it should be noted that further increases in emitter resistivities may require tighter control of spatial uniformity even in non-concentrating systems.

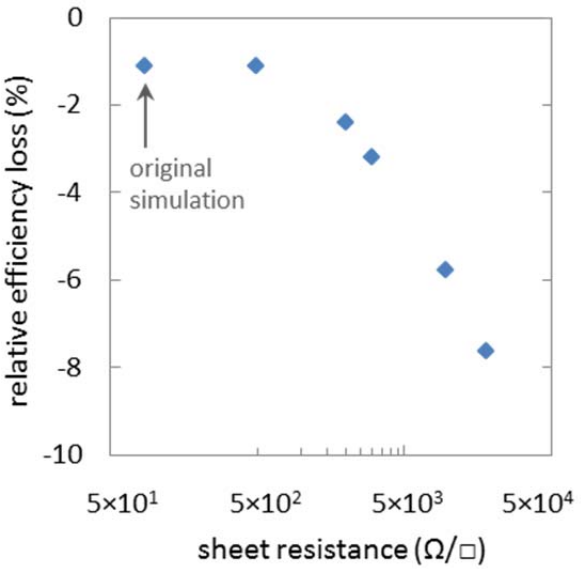

Fig. 7. Devices with high-resistance emitters are sensitive to spatial variation of light intensity. Relative efficiency reduction of a 600 μm-wide diffused junction Si cell with modified doping profiles under illumination by a split solar spectrum with fidelities of 100% in both spectral bands and *CV* of 0.009 plotted *vs.* emitter sheet resistance. Efficiency reduction is shown as a percentage of the efficiency of the same device under uniform illumination by a perfectly split solar spectrum.

C. *Analysis Limitations*

We note several limitations to the scope of this analysis. We neglect local heating effects and (since our simulations were two-dimensional) current redistribution through the metallization grid. Further, we simulate single-junction sub-cells under 1-sun illumination conditions. For effects particular to concentrated sunlight and stacked multijunction devices—resistive effects, local current mismatches, and increased resistivity of tunnel junctions—the reader is referred to [44], [47]–[49].

Because we observe almost no impact of spatial variation,

we are not able to test the efficacy of *CV* in capturing the key elements of spatial variation that do affect cell performance, for example in concentrating systems. As a general parameter, it has the disadvantage of applying only to normally distributed intensity variation. We suggest that a single quantifiable variable that captures these effects would benefit the community for considering the effects observed with concentrating optics, stacked multijunction devices, and very high resistivity emitters.

VI. Conclusions

We suggest that the spectral splitting PV community can benefit from applying sensitivity analysis to determine the key characteristics of efficient spectral splitting optics. We demonstrate its utility by evaluating two general, quantifiable parameters for spectral splitting optics: 1) spectral fidelity to measure the precision of the splitting; and 2) spatial uniformity to measure the variation of light intensity over the surface of the solar cell. Because we are performing a sensitivity analysis rather than an optimization, we use a numerical solver for our device simulations rather than a diode model, as is typical. In our TCAD simulations of Si/Cu_2O spectral splitting structures, maximizing the spectral fidelity of the lower energy band is critical, but maximizing the energy of the high-energy band is not. That is, maximizing current is critical but maximizing the voltage at which electrons are extracted is not. Our results show that in cases where changes in current are large or the injection-level dependence of voltage and fill factor are small, a diode model does capture the key effects.

We also show that low quantum efficiency can outweigh the increased voltage when determining which material should ideally absorb photons at a given wavelength. Essentially, the cross-over point in the spectral response functions of two materials may not correspond to the band gap of the wider gap material. These results suggest that materials with high quantum efficiency over only a fraction of the spectral range in which they absorb light could be used effectively in a spectral splitting scheme, possibly lowering the barrier for commercialization of novel materials. Systems with a greater number of unique absorbers may be more sensitive to the energy at which photons are extracted, and we suggest further study in this area.

We find almost no impact of spatial non-uniformity for devices with reasonably conductive emitters under 1 sun (*i.e.*, non-concentrating) illumination. The physical origin of this result in the simulations, the nearly lossless redistribution of carriers through low-resistivity emitters, agrees with earlier work on concentrating and stacked multijunction devices.

For all our simulations, we assume the spectral fidelity and spatial uniformity to be independent parameters. In reality, many optical systems exhibit chromatic aberration, with the spectral quality of light changing in space. Investigating the effects of the coupled variables may be important for some systems, especially those in which spatial variation of carrier generation has a stronger effect on performance.

Acknowledgment

D. Berney Needleman thanks Drs. Ted Bloomstein, Gary Swanson, and William Ross (Lincoln Laboratory) for instigating work on this topic and providing feedback on important considerations for optical system designers, as well as Dr. Hannes Wagner (MIT) for advice about numerical implementation of the Sentaurus Device models.

References

[1] M. A. Green, K. Emery, Y. Hishikawa, W. Warta, and E. D. Dunlop, “Solar cell efficiency tables (version 44),” *Prog. Photovolt. Res. Appl.*, vol. 22, no. 7, pp. 701–710, Jul. 2014.

[2] M. A. Green and A. Ho-Baillie, “Forty three per cent composite split-spectrum concentrator solar cell efficiency,” *Prog. Photovolt. Res. Appl.*, vol. 18, no. 1, pp. 42–47, Jan. 2010.

[3] A. Mojiri, R. Taylor, E. Thomsen, and G. Rosengarten, “Spectral beam splitting for efficient conversion of solar energy—A review,” *Renew. Sustain. Energy Rev.*, vol. 28, pp. 654–663, Dec. 2013.

[4] H. A. Atwater, M. D. Escarra, C. N. Eisler, E. D. Kosten, E. C. Warmann, S. Darbe, J. Lloyd, and C. Flowers, “Full spectrum ultrahigh efficiency photovoltaics,” in *Photovoltaic Specialists Conference (PVSC), 2013 IEEE 39th*, 2013, pp. 1631–1634.

[5] J. D. McCambridge, M. A. Steiner, B. L. Unger, K. A. Emery, E. L. Christensen, M. W. Wanlass, A. L. Gray, L. Takacs, R. Buelow, T. A. McCollum, J. W. Ashmead, G. R. Schmidt, A. W. Haas, J. R. Wilcox, J. Van Meter, J. L. Gray, D. T. Moore, A. M. Barnett, and R. J. Schwartz, “Compact spectrum splitting photovoltaic module with high efficiency,” *Prog. Photovolt. Res. Appl.*, vol. 19, no. 3, pp. 352–360, May 2011.

[6] J. C. Goldschmidt, C. Do, M. Peters, and A. Goetzberger, “Spectral splitting module geometry that utilizes light trapping,” *Sol. Energy Mater. Sol. Cells*, vol. 108, pp. 57–64, Jan. 2013.

[7] B. Mitchell, G. Peharz, G. Siefer, M. Peters, T. Gandy, J. C. Goldschmidt, J. Benick, S. W. Glunz, A. W. Bett, and F. Dimroth, “Four-junction spectral beam-splitting photovoltaic receiver with high optical efficiency,” *Prog. Photovolt. Res. Appl.*, vol. 19, no. 1, pp. 61–72, Jan. 2011.

[8] A. Barnett, D. Kirkpatrick, C. Honsberg, D. Moore, M. Wanlass, K. Emery, R. Schwartz, D. Carlson, S. Bowden, D. Aiken, A. Gray, S. Kurtz, L. Kazmerski, M. Steiner, J. Gray, T. Davenport, R. Buelow, L. Takacs, N. Shatz, J. Bortz, O. Jani, K. Goossen, F. Kiamilev, A. Doolittle, I. Ferguson, B. Unger, G. Schmidt, E. Christensen, and D. Salzman, “Very high efficiency solar cell modules,” *Prog. Photovolt. Res. Appl.*, vol. 17, no. 1, pp. 75–83, Jan. 2009.

[9] K. C. Charles, J. R. Wilcox, and J. L. Gray, “Optimization tool for multijunction photovoltaic systems,” in *Photovoltaic Specialist Conference (PVSC), 2014 IEEE 40th*, 2014, pp. 0465–0470.

[10] C. N. Eisler, E. D. Kosten, E. C. Warmann, and H. . Atwater, “Spectrum splitting photovoltaics: Polyhedral specular reflector design for ultra-high efficiency modules,” in *Photovoltaic Specialists Conference (PVSC), 2013 IEEE 39th*, 2013, pp. 1848–1851.

[11] M. D. Escarra, S. Darbe, E. C. Warmann, and H. . Atwater, "Spectrum-splitting photovoltaics: Holographic spectrum splitting in eight-junction, ultra-high efficiency module," in *Photovoltaic Specialists Conference (PVSC), 2013 IEEE 39th*, 2013, pp. 1852–1855.
[12] J. M. Russo, D. Zhang, M. Gordon, S. Vorndran, Y. Wu, and R. K. Kostuk, "Spectrum splitting metrics and effect of filter characteristics on photovoltaic system performance," *Opt. Express*, vol. 22, no. S2, p. A528, Mar. 2014.
[13] J. M. Russo, S. Vorndran, Y. Wu, and R. K. Kostuk, "Cross-correlation analysis of dispersive spectrum splitting techniques for photovoltaic systems," *J. Photonics Energy*, vol. 5, no. 1, pp. 054599–054599, 2015.
[14] A. G. Imenes and D. R. Mills, "Spectral beam splitting technology for increased conversion efficiency in solar concentrating systems: a review," *Sol. Energy Mater. Sol. Cells*, vol. 84, no. 1–4, pp. 19–69, Oct. 2004.
[15] J. A. Cape, J. S. Harris, and R. Sahai, "Spectrally split tandem cell converter studies," in *Proceedings of the 13th IEEE Photovoltaic Specialists Conference*, Washington, DC, 1978, pp. 881–885.
[16] P. G. Borden, P. E. Gregory, O. E. Moore, H. Vander Plas, and L. W. James, "A 10-unit dichroic filter spectral splitter module," in *Proceedings of the 15th IEEE Photovoltaic Specialists Conference*, Kissimmee, FL, 1981, pp. 311–316.
[17] E. D. Kosten, J. Lloyd, E. Warmann, and H. . Atwater, "Spectrum splitting photovoltaics: Light trapping filtered concentrator for ultrahigh photovoltaic efficiency," in *Photovoltaic Specialists Conference (PVSC), 2013 IEEE 39th*, 2013, pp. 3053–3057.
[18] C. Wadia, A. P. Alivisatos, and D. M. Kammen, "Materials Availability Expands the Opportunity for Large-Scale Photovoltaics Deployment," *Environ. Sci. Technol.*, vol. 43, no. 6, pp. 2072–2077, Mar. 2009.
[19] D. M. Powell, M. T. Winkler, H. J. Choi, C. B. Simmons, D. B. Needleman, and T. Buonassisi, "Crystalline silicon photovoltaics: a cost analysis framework for determining technology pathways to reach baseload electricity costs," *Energy Environ. Sci.*, vol. 5, no. 3, pp. 5874–5883, Mar. 2012.
[20] ITRPV Working Group, "International Technology Roadmap for Photovoltaic (ITRPV): 2013 Results, Revision 1," SEMI PV Group, Mar. 2014.
[21] C. H. Henry, "Limiting efficiencies of ideal single and multiple energy gap terrestrial solar cells," *J. Appl. Phys.*, vol. 51, no. 8, p. 4494, 1980.
[22] Y. S. Lee, M. Bertoni, M. K. Chan, G. Ceder, and T. Buonassisi, "Earth abundant materials for high efficiency heterojunction thin film solar cells," in *2009 34th IEEE Photovoltaic Specialists Conference (PVSC)*, 2009, pp. 002375–002377.
[23] A. Feltrin and A. Freundlich, "Material considerations for terawatt level deployment of photovoltaics," *Renew. Energy*, vol. 33, no. 2, pp. 180–185, Feb. 2008.
[24] T. Minami, Y. Nishi, T. Miyata, and J. Nomoto, "High-Efficiency Oxide Solar Cells with ZnO/Cu2O Heterojunction Fabricated on Thermally Oxidized Cu2O Sheets," *Appl. Phys. Express*, vol. 4, no. 6, p. 062301, Jun. 2011.
[25] T. Minami, T. Miyata, K. Ihara, Y. Minamino, and S. Tsukada, "Effect of ZnO film deposition methods on the photovoltaic properties of ZnO–Cu2O heterojunction devices," *Thin Solid Films*, vol. 494, no. 1–2, pp. 47–52, Jan. 2006.
[26] "NREL Efficiency Chart." [Online]. Available: http://www.nrel.gov/ncpv/images/efficiency_chart.jpg. [Accessed: 18-Feb-2015].
[27] Y. S. Lee, D. Chua, R. E. Brandt, S. C. Siah, J. V. Li, J. P. Mailoa, S. W. Lee, R. G. Gordon, and T. Buonassisi, "Atomic Layer Deposited Gallium Oxide Buffer Layer Enables 1.2 V Open-Circuit Voltage in Cuprous Oxide Solar Cells," *Adv. Mater.*, vol. 26, no. 27, pp. 4704–4710, Jul. 2014.
[28] S. C. Siah, M. Lloyd, S. Johnston, R. E. Brandt, Y. S. Lee, and T. Buonassisi, "Achieving a High 10 μs μ-PCD Carrier Lifetime in Cuprous Oxide (Cu2O) by Bulk Defect Engineering," presented at the MRS Spring Meeting, San Francisco, CA, 2014.
[29] Y. S. Lee, M. T. Winkler, S. Cheng Siah, R. Brandt, and T. Buonassisi, "High-mobility copper (I) oxide thin films prepared by reactive dc magnetron sputtering for photovoltaic applications," in *2011 37th IEEE Photovoltaic Specialists Conference (PVSC)*, 2011, pp. 000250–000251.
[30] Y. S. Lee, M. T. Winkler, S. Cheng Siah, R. Brandt, and T. Buonassisi, "Growth and p-type doping of cuprous oxide thin-films for photovoltaic applications," in *2012 38th IEEE Photovoltaic Specialists Conference (PVSC)*, 2012, pp. 002557–002558.
[31] S. C. Siah, Y. S. Lee, Y. Segal, and T. Buonassisi, "Low contact resistivity of metals on nitrogen-doped cuprous oxide (Cu2O) thin-films," *J. Appl. Phys.*, vol. 112, no. 8, p. 084508, Oct. 2012.
[32] J. Zhao, A. Wang, and M. A. Green, "24·5% Efficiency silicon PERT cells on MCZ substrates and 24·7% efficiency PERL cells on FZ substrates," *Prog. Photovolt. Res. Appl.*, vol. 7, no. 6, pp. 471–474, Nov. 1999.
[33] J. Zhao, A. Wang, and M. A. Green, "24.5% efficiency PERT silicon solar cells on SEH MCZ substrates and cell performance on other SEH CZ and FZ substrates," *Sol. Energy Mater. Sol. Cells*, vol. 66, no. 1–4, pp. 27–36, Feb. 2001.
[34] J. Zhao, A. Wang, and M. A. Green, "High-efficiency PERL and PERT silicon solar cells on FZ and MCZ substrates," *Sol. Energy Mater. Sol. Cells*, vol. 65, no. 1–4, pp. 429–435, Jan. 2001.
[35] D. D. Smith, P. J. Cousins, A. Masad, S. Westerberg, M. Defensor, R. Ilaw, T. Dennis, R. Daquin, N. Bergstrom, A. Leygo, X. Zhu, B. Meyers, B. Bourne, M. Shields, and D. Rose, "SunPower's Maxeon Gen III solar cell: High efficiency and energy yield," in *Photovoltaic Specialists Conference (PVSC), 2013 IEEE 39th*, 2013, pp. 0908–0913.
[36] M. Taguchi, A. Yano, S. Tohoda, K. Matsuyama, Y. Nakamura, T. Nishiwaki, K. Fujita, and E. Maruyama, "24.7% Record Efficiency HIT Solar Cell on Thin Silicon Wafer," *IEEE J. Photovolt.*, vol. 4, no. 1, pp. 96–99, Jan. 2014.
[37] R. E. Brandt, "Elucidating efficiency losses in cuprous oxide (Cu_2O) photovoltaics and identifying strategies for efficiency improvement," Thesis, Massachusetts Institute of Technology, 2013.
[38] T. Minami, Y. Nishi, and T. Miyata, "High-Efficiency Cu_2O-Based Heterojunction Solar Cells Fabricated Using a Ga_2O_3 Thin Film as N-Type Layer," *Appl. Phys. Express*, vol. 6, no. 4, p. 044101, Apr. 2013.

[39] D. Berney Needleman, "Optical Design Guidelines for Spectral Splitting Photovoltaic Systems: A Sensitivity Analysis Approach," M.S., Massachusetts Institute of Technology, Cambridge, MA, USA, 2014.
[40] Y. S. Lee, J. Heo, S. C. Siah, J. P. Mailoa, R. E. Brandt, S. B. Kim, R. G. Gordon, and T. Buonassisi, "Ultrathin amorphous zinc-tin-oxide buffer layer for enhancing heterojunction interface quality in metal-oxide solar cells," *Energy Environ. Sci.*, vol. 6, no. 7, pp. 2112–2118, Jun. 2013.
[41] C. N. Eisler, Z. R. Abrams, M. T. Sheldon, X. Zhang, and H. A. Atwater, "Multijunction solar cell efficiencies: effect of spectral window, optical environment and radiative coupling," *Energy Env. Sci*, Sep. 2014.
[42] J. M. Castro, D. Zhang, B. Myer, and R. K. Kostuk, "Energy collection efficiency of holographic planar solar concentrators," *Appl. Opt.*, vol. 49, no. 5, pp. 858–870, Feb. 2010.
[43] G. Kim, J. A. Dominguez-Caballero, H. Lee, D. J. Friedman, and R. Menon, "Increased Photovoltaic Power Output via Diffractive Spectrum Separation," *Phys. Rev. Lett.*, vol. 110, no. 12, p. 123901, Mar. 2013.
[44] I. García, P. Espinet-González, I. Rey-Stolle, and C. Algora, "Analysis of Chromatic Aberration Effects in Triple-Junction Solar Cells Using Advanced Distributed Models," *IEEE J. Photovolt.*, vol. 1, no. 2, pp. 219–224, Oct. 2011.
[45] A. Cuevas and S. López-Romero, "The combined effect of non-uniform illumination and series resistance on the open-circuit voltage of solar cells," *Sol. Cells*, vol. 11, no. 2, pp. 163–173, Mar. 1984.
[46] A. Vishnoi, R. Gopal, R. Dwivedi, and S. K. Srivastava, "Combined effect of non-uniform illumination and surface resistance on the performance of a solar cell," *Int. J. Electron.*, vol. 66, no. 5, pp. 755–774, 1989.
[47] E. Franklin and J. Coventry, "Effects of highly non-uniform illumination distribution on electrical performance of solar cells," 2004.
[48] A. Luque and V. M. Andreev, *Concentrator photovoltaics*. Berlin: Springer, 2007.
[49] H. Baig, K. C. Heasman, and T. K. Mallick, "Non-uniform illumination in concentrating solar cells," *Renew. Sustain. Energy Rev.*, vol. 16, no. 8, pp. 5890–5909, Oct. 2012.

David Berney Needleman received the B.S. degree in physics from the University of Oregon, Eugene, OR, USA, in 2007 and the M.S. degree in mechanical engineering from the Massachusetts Institute of Technology, Cambridge, MA, USA, in 2014, where he is currently working toward the Ph.D. degree in mechanical engineering.

He was a Research and Development Engineer with Atlantic Solar, Cape Town, South Africa. His current research interests include structural defects in crystalline silicon solar cells.

Jonathan P. Mailoa received the B.S. and M.Eng. degrees from the Massachusetts Institute of Technology, Cambridge, MA, USA, where he is currently working toward the Ph.D. degree.

He is doing research on multijunction-on-silicon solar cell in an effort to push efficiency of silicon-based solar cells beyond its fundamental single-junction efficiency limit. His research interests include optical simulation in thin-film structures, as well as designing novel device architectures for PV systems.

Riley E. Brandt received the B.S. degree in mechanical engineering in 2011, and the M.S. degree in mechanical engineering in 2013 from the Massachusetts Institute of Technology, Cambridge, MA, USA where he is currently a Ph.D. candidate.

His current research interests include engineering thin-film PV devices based on novel, Earth-abundant absorbers, and diagnosing their efficiency loss mechanisms to accelerate development.

Niall M. Mangan received the Ph.D. degree in systems biology from Harvard University, Cambridge, MA, USA in 2013, and the B.S. degree in physics and mathematics from Clarkson University, Potsdam, NY, USA.

She is a postdoctoral associate in the Photovoltaic Research Laboratory, Massachusetts Institute of Technology, Cambridge, MA, USA. Her current research interests include device modeling to enhance the development of Earth-abundant thin film photovoltaics, carrier selective contacts, and measurement interpretation.

Tonio Buonassisi received the Ph.D. degree in applied science and technology from the University of California at Berkeley, Berkeley, CA, USA, with additional research at the Fraunhofer Institute for Solar Energy Systems and the Max-Planck-Institute for Microstructure Physics.

He is the Head of the Photovoltaic Research Laboratory, Massachusetts Institute of Technology, Cambridge, MA, USA, which combines crystal growth, processing, characterization, defect simulation, and cost-performance modeling to engineer naturally abundant and manufacturable materials into cost-effective, high-performance devices. His research interests include

silicon (kerfless absorbers, advanced manufacturing, and defects), Earth-abundant thin films, and high-efficiency concepts.